Hindawi
Advances in Civil Engineering
Volume 2021, Article ID 6832188, 11 pages
https://doi.org/10.1155/2021/6832188

Research Article

Calculation Model of Shear Capacity of Multiple Composite Core Column Joints Based on Softened Tension-Compression Bar Model

Xu Wentao[1] **and Yang Chengyu**[2]

[1]*College of Architecture and Engineering, Xinjiang University, Urumqi 830047, China*
[2]*Chengdu Benchmark Fangzhong Architectural Design Co., Ltd., Chengdu, China*

Correspondence should be addressed to Xu Wentao; cpsrgusu@163.com

Received 7 July 2021; Accepted 13 August 2021; Published 1 September 2021

Academic Editor: Zhiyong Chen

This paper aims to study the seismic performance of multiple composite core column joints. The influence of the stress mechanism, axial compression ratio, and shear span ratio on the failure mode, hysteretic performance, and shear capacity of the multiple composite core column joints was studied through the low-reversed cyclic loading tests of three specially designed and manufactured multiple composite core column joints. The angle ratio method is used to calculate the effective area of the vertical tie bar, and based on the mechanism of the softening tension-compression bar, the formula for calculating the shear capacity of the joint with multiple composite core column is established. In addition, it is also verified by the test data in this paper. The experimental results show that when the axial compression ratio increases from 0.26 to 0.45, the number and width of cracks at the beam end decrease. When the shear span ratio increases from 1.67 to 2.22, the number and width of cracks at the joint beam end increase. The average value and standard deviation of the ratio between the measured value and the calculated value of the shear capacity are 0.97 and 0.16, indicating that the proposed calculation method has a high agreement with the actual value and strong engineering application.

1. Introduction

Beam-column joints play an important role in the transmission and distribution of internal forces and are also the key to the seismic performance of the structure in the frame structure. Most of the ordinary reinforced concrete beam-column joints show brittle failure, which is not conducive to the seismic resistance of the structure [1–3]. To explore a new type of reinforcement and improve the transmission and distribution of internal forces in the frame, much attention has been paid by researchers. In recent years, multiple composite reinforced core columns can effectively guarantee the realization of "strong column and weak beam" and have good shear bearing capacity and seismic performance under earthquake action, which has attracted increasing attention of researchers. As the core index of seismic shear capacity is particularly important, many researchers have done a series of studies on it [4–12].

You et al. [13] comprehensively analyzed the seismic tests of numerous international frame joints, found the important correlation between the stress state of longitudinal bars after yield and the number of longitudinal bars that affect the shear capacity of joints, and proposed the shear capacity formula of such failure-type joints. Xing et al. [14–16] proposed a modified calculation model for reinforced concrete joints with orthogonal beams on the basis of the model of softened tension-compression bars [17, 18]. Yang [19] studied the influence of axial compression ratio, stirrup spacing, stirrup ratio, and stirrup form on the seismic performance of multiple composite core columns and proposed the corresponding calculation formula of shear capacity and design suggestions. Wakabayshi et al. [20] and Omine et al. [21] found that the seismic performance of cored columns was significantly better than that of ordinary reinforced concrete columns in their studies under low-cyclic reciprocating loads. Kadoya et al. [22] found that the

initial stiffness and strength of columns with core columns are about 1.2 times that of ordinary reinforced concrete columns. At present, most of the joint researches at home and abroad are made of reinforced concrete beam-column joints in the form of ordinary reinforcement. Although the research on the seismic performance of composite core columns has made some progress, there are few reports on the seismic performance of composite core columns, especially the calculation of its shear capacity needs to be further studied.

Based on the above analysis, this paper carried out pseudostatic tests on the beam-column joints composed of multiple composite core columns, analyzed the effects of axial compression ratio and shear span ratio on the seismic performance of the joints, and proposed a formula for calculating the shear capacity of the multiple composite core column joints based on the mechanism of softening the tension and compression rods. It provides reference for the popularization and use of such nodes in engineering construction.

2. Materials and Methods

To avoid the contingency caused by single data, three reinforced concrete beam joints with multiple composite core columns were prepared for parallel tests. The beam section size of each node is 150 mm × 380 mm, the column section size is 400 mm × 400 mm, and the concrete protective layer thickness of the beam and column is 20 mm. The specimens BCJ-1, BCJ-2, and BCJ-3 were designed and manufactured with axial compression ratio and shear span ratio as variables. Specific joint dimensions and reinforcement can be found in Figures 1 and 2 and Table 1.

The measured compressive strength of concrete cube used in the test is 58.6 MPa, and the measured material properties of steel bars with different diameters are shown in Table 2.

The static loading method is used as shown in Figure 3 in the experiment of this paper. The loading process is mainly divided into the following two steps:

(1) Vertical load was applied to the top of the node column by a hydraulic Jack.

The first application of axial pressure is 0.4 times to ensure that the device is not loosened, and then two further cycles of 0.4 times. Finally, the axial pressure applied at the top of the column is 1 time and remains constant.

(2) Horizontal displacement load is applied to the joint column end through the actuator.

Before the formal loading, 5 kN force was used to push and pull the joint specimen three times for trial loading to ensure the normal working of each device, acquisition system, and fixed device. After the complete system is tested to work normally, the horizontal load is returned to 0. The step size of initial loading of horizontal displacement is 2 mm, 4 mm, 6 mm, 8 mm, and 10 mm in turn, and then the step size remains 10 mm. Each step size is repeated three times until the specimen is damaged or the horizontal load is less than 0.85 times the peak load, and the loading is finished. The vibration frequency of the load is the simulated seismic load, as shown in Figure 4.

3. Results and Discussion

3.1. Phenomena and Failure Modes. For multiple composite core column joints, the frame columns are always in the elastic stage, and the core areas of the columns and joints have no obvious damage under the reciprocating action of horizontal displacement loads. With the loading process, penetration cracks appear at the beam-column junction, and cross oblique cracks appear at the beam end away from the edge of the column. Concrete in this area gradually spall off with the subsequent loading, and obvious plastic failure occurs at the edge of the beam away from the column. The failure modes of each specimen are shown in Figures 5 to 7.

It can be found that the number and width of cracks at the beam end decrease as the axial compression ratio increases from 0.26 (node BCJ-1) to 0.45 (node BCJ-2) when the specimen is damaged. However, the horizontal displacement of failure is just the opposite. The horizontal displacement of BCJ-1 node is 70 mm, while that of BCJ-2 node is 50 mm. This is because the increase of axial compression ratio will cause the concrete at the core of the joint to be subjected to greater compression, so as to delay the generation of cracks at the beam and column ends at the core of the joint. It is shown that increasing the axial compression ratio can delay the development of the beam end cracks but reduce the ductility of the joint under seismic load. Similarly, when the shear-span ratio increases from 1.67 (node BCJ-1) to 2.22 (node BCJ-3), the number and width of fractures at the joints increase. This is because when the shear span ratio increases, the second-order effect of joints becomes more obvious, which intensifies the generation and development of beam-end cracks. For details, see the red mark in the revised manuscript. Increasing the shear-span ratio will accelerate the generation of fractures at the joints.

3.2. Hysteretic Behavior. The hysteretic curves of each specimen are shown in Figures 8 to 10. In the early stage of loading, the hysteretic loop area and residual deformation of each joint are small, and the stiffness degradation of the specimen is not obvious. The area and residual deformation of the hysteresis loop gradually increase with the increase of the load. When the horizontal displacement load reaches its peak, the stiffness of the joint degrades obviously. With the continuous loading, the hysteresis loop area of the curve increases, the maximum load at all levels begins to decrease, and the rising part of the curve tends to be gentle. The hysteresis curves of the three specimen nodes all show a spindle shape without obvious pinching, and the load strength and specimen stiffness do not significantly degrade when the load of the same level is loaded each time. The cumulative damage of the frame joints under cyclic loads at

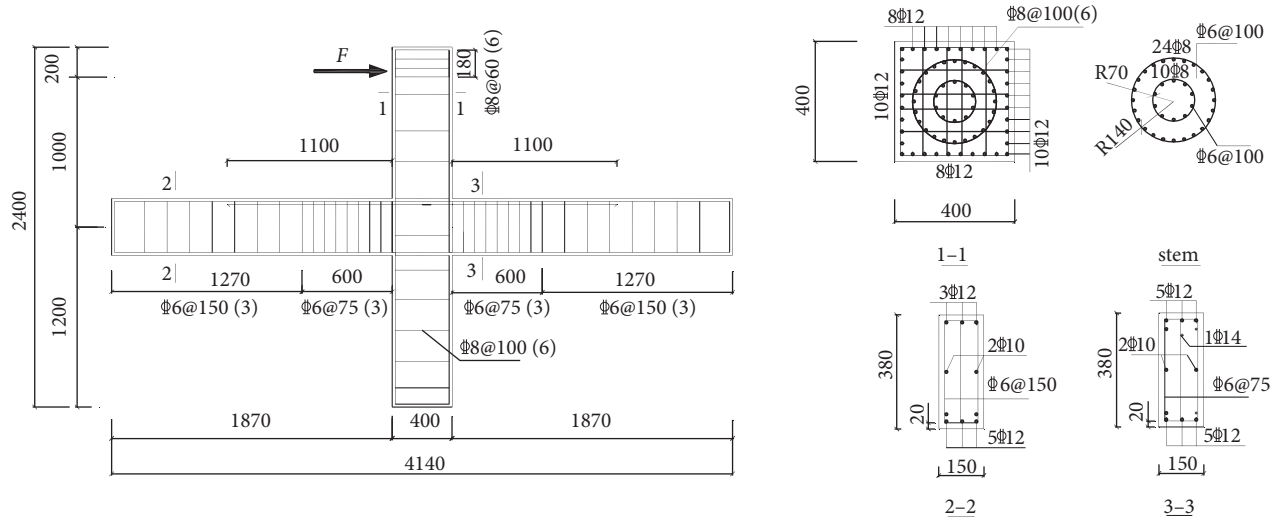

Figure 1: Detailed drawing of reinforcement for BCJ-1 (BCJ-2) joints.

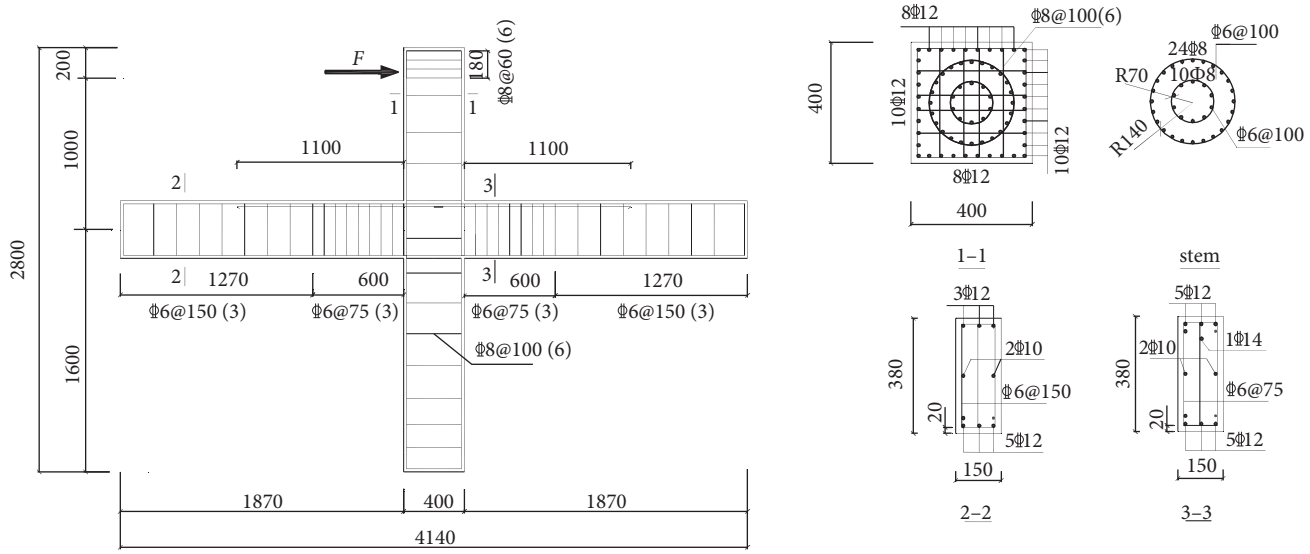

Figure 2: Detailed drawing of reinforcement for BCJ-3 joints.

all levels is small, and the residual deformation of the joints under cyclic loads at all levels is uniform after the peak load. However, the load-displacement hysteresis curves of the beam-column joints with common reinforcement form mostly present bow and inverse "S" shape [23–25], which proves that the multicomposite core column joints have better seismic performance than the beam-column joints with common reinforcement form.

Skeleton curve of the node refers to the line between the first loading curve of the node and the peak points of hysteretic loops in the hysteretic loop curve under the action of low-cycle reciprocating load. The skeleton curve drawn by the line of the peak points of each hysteretic loop under low-cycle reciprocating load is shown in Figure 11. The initial stiffness of the frame joints increases by about 21.6 kN/mm, and the peak load increases by about 103.5 kN, when the axial compression ratio increases from 0.26 to 0.45. As for the effect of the shear to span ratio, the initial stiffness of the node decreases by about 1.3 kN/mm and the peak value by about 22.9 kN, when the shear to span ratio increases from 1.67 to 2.22. The results show that the increase of axial compression ratio can significantly increase the initial stiffness and peak load of the composite core column joints, while the shear span ratio is just the opposite.

3.3. Calculation of Horizontal Shear Stress on Nodes. The force analysis of nodes is shown in Figure 12.

The upper half of the node is taken as the isolation body, and the horizontal shear force of the node has the following equilibrium relationship:

$$V_{jh} = T_{b1} + C_{b2} - V_{c1}. \quad (1)$$

According to the geometric relationship, the vertical shear force of the node is

Table 1: The detailed parameters of the frame node in test.

Project			BCJ-1	BCJ-2	BCJ-3
Mandrel	Rectangular frame column	Section (mm × mm)	400 × 400	400 × 400	400 × 400
		Angle steel	4Φ12	4Φ12	4Φ12
		Unilateral longitudinal bars	10Φ12+8Φ12	10Φ12+8Φ12	10Φ12+8Φ12
		Stirrup	Φ8@100[6 limbs]	Φ8@100[6limbs]	Φ8@100[6limbs]
	Outer mandrel XZ-1	Section (mm × mm)	280×280(circle)	280×280(circle)	280×280(circle)
		Longitudinal bars	24Φ8	24Φ8	24Φ8
		Stirrup	Φ6@100	Φ6@100	Φ6@100
	Inner mandrel XZ-2	Section (mm × mm)	140 × 140 (circle)	140 × 140 (circle)	140 × 140 (circle)
		Longitudinal bars	10Φ8	10Φ8	10Φ8
		Stirrup	Φ6@100	Φ6@100	Φ6@100
Strength of concrete (MPa)			C45	C45	C45
Axial pressure (kN)			1560	2750	1560
Lower column height			2.4	2.4	3.2
Height of reverse bending point of lower column			1.2	1.2	1.6
Height of upper column			1.9	1.9	1.9
Height of upper column reverse bending point			1.0	1.0	1.0
Experimental axial compression ratio			0.26	0.45	0.26
Shear span ratio			1.67	1.67	2.22
Beam	Section (mm × mm)		150 × 380	150 × 380	150 × 380
	Concrete strength (MPa)		C45	C45	C45
	Stirrup		Φ6@75/150(3)	Φ6@75/150(3)	Φ6@75/150(3)
	Beam length (m)		3.75	3.75	3.75
	Length of reverse bending point (m)		1.87	1.87	1.87
	Midspan compression bars		3Φ12	3Φ12	3Φ12
	Negative bending regions		5Φ12+1Φ14	5Φ12+1Φ14	5Φ12+1Φ14
	Lower longitudinal bars		5Φ12	5Φ12	5Φ12
	Longitudinal bars		2Φ10	2Φ10	2Φ10

Table 2: Property of steel bars.

Diameter (mm)	Yield strength f_y (N/mm^2)	Ultimate strength f_u (N/mm^2)	Elastic modulus E_s (N/mm^2)
6	434.60	605.20	2.0×10^5
8	539.70	706.70	2.0×10^5
10	490.24	659.45	2.0×10^5
12	484.20	624.90	2.0×10^5
14	455.10	639.45	2.0×10^5

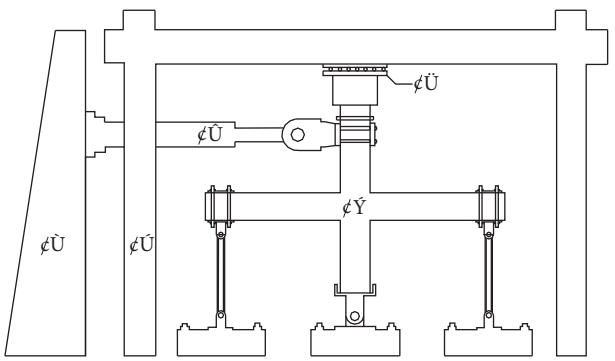

Figure 3: Schematic diagram of loading device. Note: ① reaction wall, ② gantry mounting, ③ MTS actuator, ④ horizontal rolling system, and ⑤ test specimen.

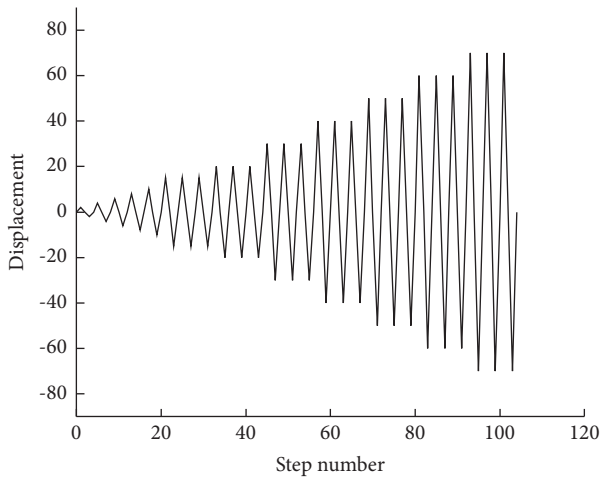

Figure 4: The vibration frequency of the load.

$$V_{jv} \approx \left(\frac{h_b'}{h_c'}\right) \times V_{jh}, \tag{2}$$

$$T_{b1} = \frac{M_{b2}}{h_b'}, \tag{3}$$

$$C_{b2} = \frac{M_{b1}}{h_b'}, \tag{4}$$

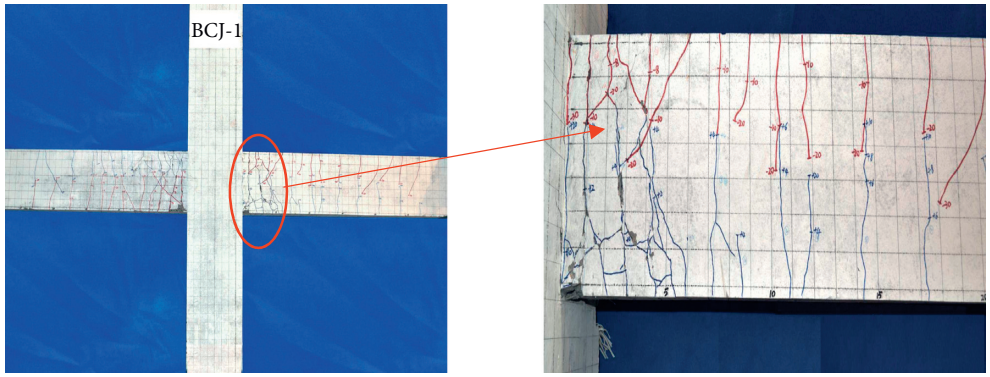

Figure 5: BCJ-1 node failure pattern diagram.

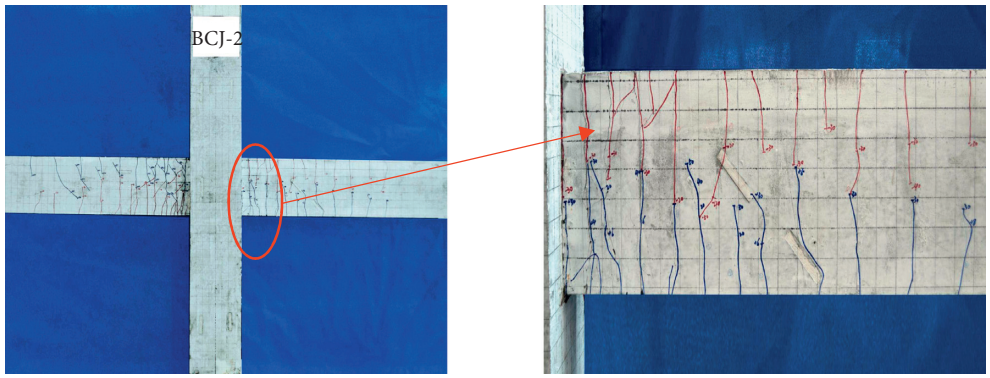

Figure 6: BCJ-2 node failure pattern diagram.

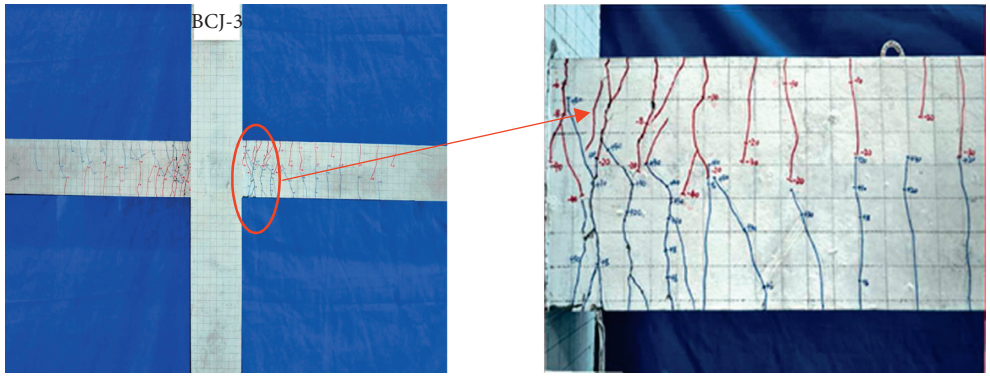

Figure 7: BCJ-3 node failure pattern diagram.

where V_{jh} is the horizontal shear force of the node, T_{b1} is the tensile force of the reinforcement of the beam on the right side of the node, and C_{b2} is the pressure of the beam on the left side.

The orientation of T_{b1} and C_{b2} is assumed to be consistent although not necessarily in the actual force, for simplicity of calculation. V_{c1} is the horizontal shear force at the column end at the node, which is equal to the load value of horizontal loading. M_{b1} and M_{b2} are the bending moments at the end of the beam; h_b' and h_c' are the internal moment arms of the beam and column, respectively, the approximate distance between the center lines of upper and lower longitudinal bars of the beam is taken to calculation the h_b'.

According to equations (1), (3), and (4), we can get

$$V_{jh} = \frac{M_{b1} + M_{b2}}{h_b'} - V_{c1}. \tag{5}$$

Balanced by the bending moment of the node, the following equation can be obtained:

$$M_{c1} + M_{c2} = M_{b1} + M_{b2}. \tag{6}$$

Among them,

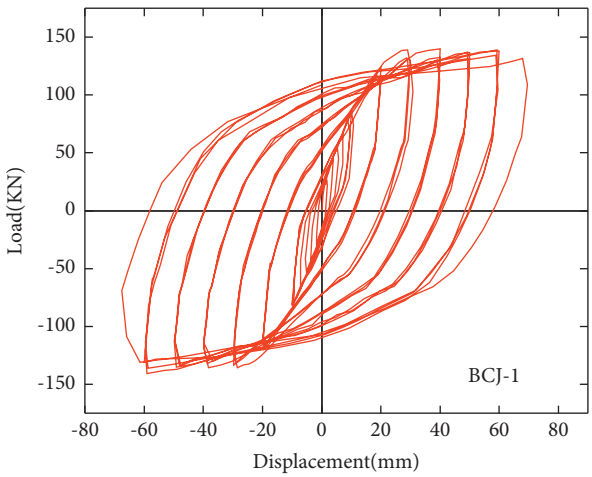

Figure 8: BCJ-1 load-displacement hysteresis curve.

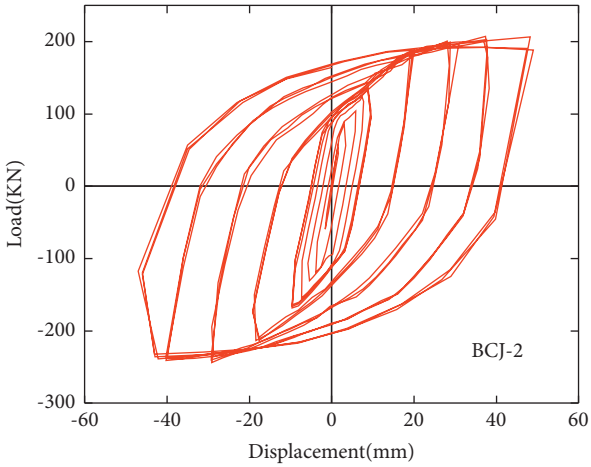

Figure 9: BCJ-2 load-displacement hysteresis curve.

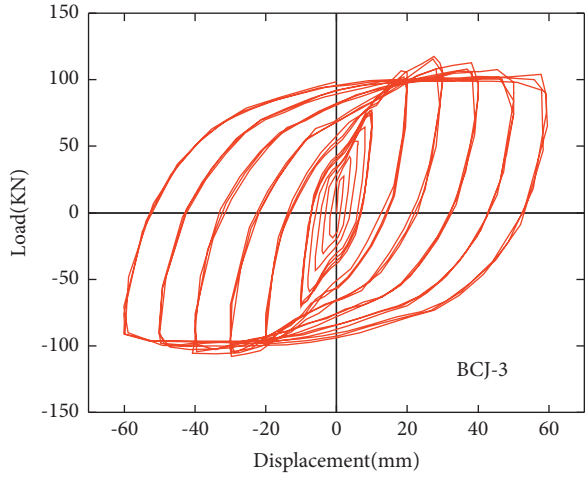

Figure 10: BCJ-3 load-displacement hysteresis curve.

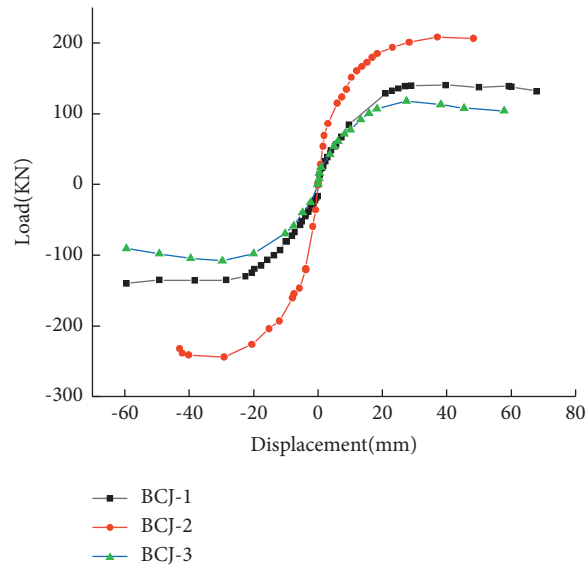

Figure 11: Comparison diagram of skeleton curve.

$$\begin{cases} M_{c1} = V_{c1}h_1, \\ M_{c2} = V_{c2}h_2, \end{cases} \tag{7}$$

$$V_{c1} = V_{c2}. \tag{8}$$

Equations (6) to (8) can be deduced as follows:

$$\begin{aligned} V_{c1} &= \frac{M_{b1} + M_{b2}}{h_1 + h_2} \\ &= \frac{M_{b1} + M_{b2}}{h - h_b}, \end{aligned} \tag{9}$$

where M_{c1} and M_{c2} are bending moments at the upper and lower column ends; h is the distance between the reverse bending points of the upper and lower columns; h_1 and h_2 are the distance between the reverse bending points of the upper and lower columns and the core area of the joint, respectively; and h_b is the height of the cross section of the beam.

By combining equations (9) and (5), we can get

$$V_{jh} = \frac{M_{b1} + M_{b2}}{h_b'}\left(1 - \frac{h_b'}{h - h_0}\right). \tag{10}$$

The shear forces on the three nodes in the horizontal direction are finally calculated, as shown in Table 3.

4. Calculation Formula of Shear Capacity Based on Softening Tension-Compression Bar Model

The complex mechanical behavior of the whole structure is abstracted into a relatively simple strut-and-tie model by taking the compression concrete as the compression struts; and the steel bar in the tension zone as the tie bar. The simplified softened strut-and-tie model is a model proposed by Professor Huang Shijian to calculate the shear capacity of beam-and-column joints on the basis of the softened strut-

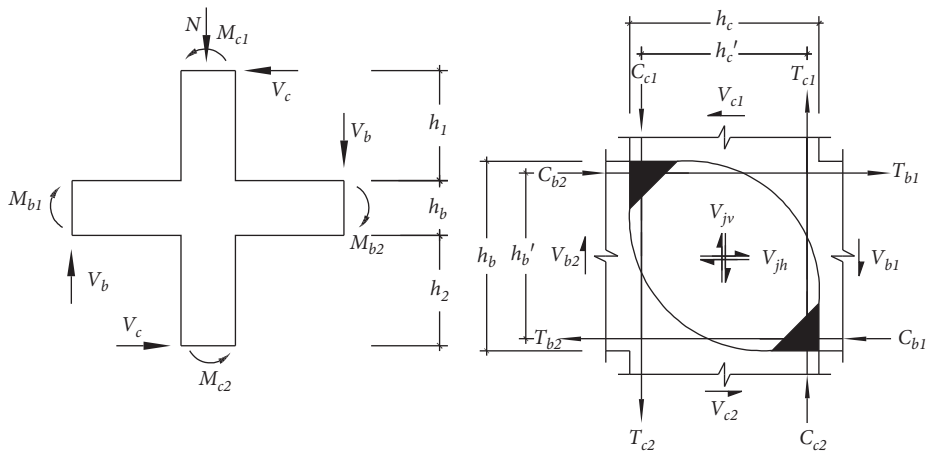

Figure 12: Schematic diagram of force of nodes: (a) diagram of external forces on node and (b) analysis of the internal forces on node.

and-tie model [26, 27]. The schematic diagram of the softened strut-and-tie model is shown in Figure 13. The model is composed of oblique, horizontal, and vertical parts. The oblique part is composed of a baroclinic bar, and the included angle between the baroclinic bar and the horizontal axis is θ; the horizontal part is composed of a horizontal tie bar and two gentle compression struts, which are composed of stirrups at the nodes; the vertical part consists of a vertical tie bar and two steep compression struts, which are composed of the longitudinal bars of the columns [15]. The specific calculation method and calculation process are as follows:

The horizontal shear bearing capacity of this model, V_j is calculated as follows:

$$V_j = K\zeta f_c' A_{str} \cos\theta, \tag{11}$$

where θ is the included angle between the baroclinic bar and the horizontal direction, which can be determined by the following equation:

$$\theta = \tan^{-1}\left(\frac{h_b''}{h_c''}\right). \tag{12}$$

For the convenience of calculation, b and c in the equation are assumed to be the distances between the center lines of the outermost reinforcement of the beam and column, respectively, and the inclination direction and magnitude of the baroclinic bar in the joint area and the main compressive stress of the concrete in the core area are considered to be the same.

The area A_{str} of the baroclinic bar can be calculated as follows:

$$A_{str} = a_s \times b_s, \tag{13}$$

where a_s and b_s are the effective height and width of the baroclinic bar, respectively, determined by the following equation:

$$a_s = \sqrt{a_b^2 + a_c^2}, \tag{14}$$

$$b_s = \min\left\{b_b + 2 \times \frac{a_c}{6}, b_c\right\}, \tag{15}$$

where a_b is the height of the compression zone of the beam cross section and a_c is the height of the compression zone of the column cross section, which can be determined by the following equation:

$$a_b = \frac{h_b}{5}, \tag{16}$$

$$a_c = \left(0.25 + 0.85\frac{N}{A_g f_c'}\right)h_c, \tag{17}$$

where b_b is the beam cross-section width, b_c is the column cross-section width, h_b is the beam cross-section height, h_c is the column cross-section height, N is the axial pressure, determined according to the test, A_g is the column cross-section area, and f_c' is the compressive strength of the concrete cylinder. According to the conversion formula of "Standard for test methods of concrete physical and mechanical properties" (GB/T50081-2019) [28], the compressive strength of the concrete cube is converted into the compressive strength of the cylinder. K is the tension/compression bar coefficient. Professor Huang Shijian [26] suggested the following equation for calculation:

$$K = K_h + K_v - 1, \tag{18}$$

where K_h is the horizontal tie bar coefficient and K_v is the vertical tie bar coefficient. The values of the two are shown in the following equation:

Table 3: The shear on the three nodes in the horizontal direction.

Specimen	BCJ-1	BCJ-2	BCJ-3
V_{jh}KN	668.71	1161.32	708.58

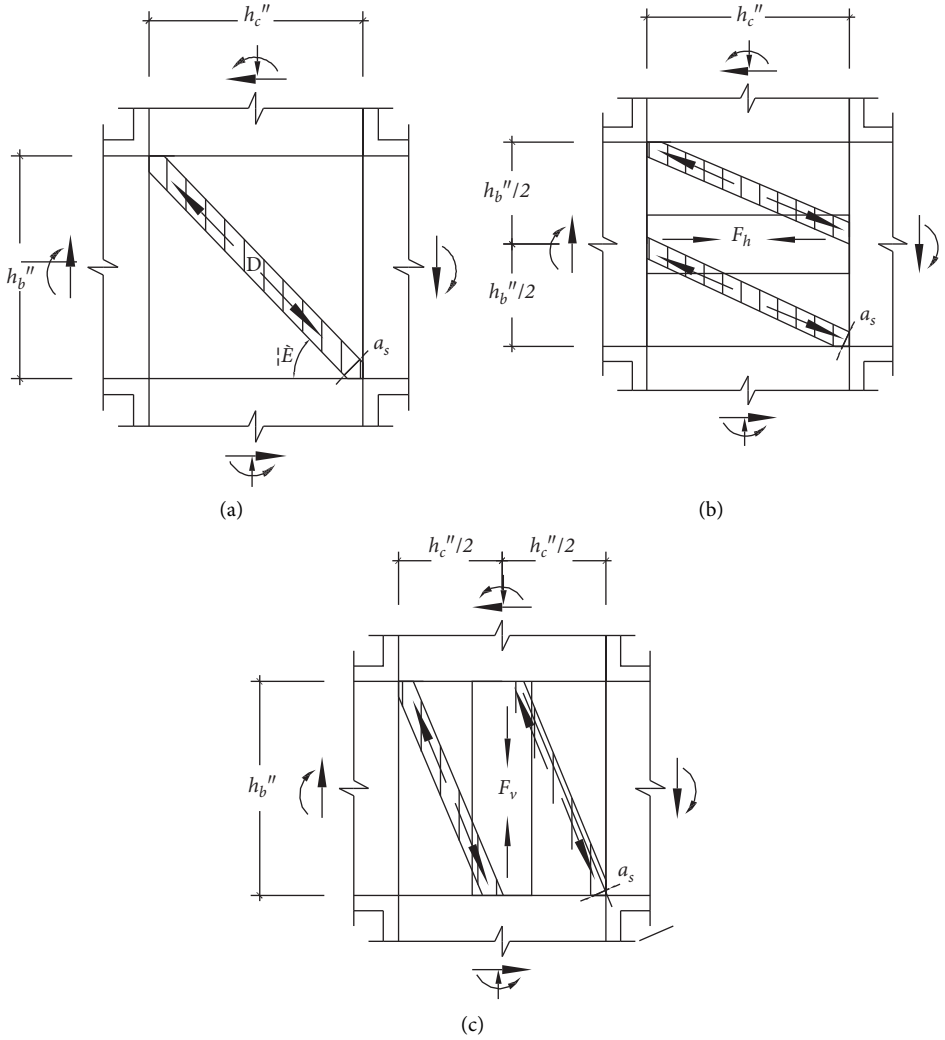

Figure 13: The strut-and-tie model of the node: (a) oblique part, (b) horizontal part, and (c) vertical part.

$$\begin{cases} K_h = 1 + \dfrac{(\overline{K_h} - 1)A_{th}f_{yh}}{\overline{F_h}} \le \overline{K_h}, \\ K_v = 1 + \dfrac{(\overline{K_v} - 1)A_{tv}f_{yv}}{\overline{F_v}} \le \overline{K_v}, \end{cases} \tag{19}$$

where $A_{th}f_{yh}$ is the product of the area of the horizontal tie bar and the yield strength of the corresponding steel bar and $A_{tv}f_{yv}$ is the product of the area of the vertical tie bar and the yield strength of the corresponding reinforcing bar. If the tie bar consists of different types of reinforcement, then $A_{th}f_{yh}$ and $A_{tv}f_{yv}$ shall be the sum of the products of different types.

$\overline{K_h}$ is the balance coefficient of the horizontal tie bar and $\overline{K_v}$ is the balance coefficient of the vertical tie bar, which can be calculated as follows:

$$\begin{cases} \overline{K_h} \approx \dfrac{1}{1 - 0.2\left(\gamma_h + \gamma_h^2\right)}, \\ \overline{K_v} \approx \dfrac{1}{1 - 0.2\left(\gamma_v + \gamma_v^2\right)}, \end{cases} \tag{20}$$

where γ_h is the ratio of the horizontal tie bar to the horizontal shear stress of the node and γ_v is the ratio of the vertical tie bar to the horizontal shear stress of the node, which can be calculated as follows:

$$\begin{cases} \gamma_h = \dfrac{2\tan\theta - 1}{3}, \\ \gamma_v = \dfrac{2\cot\theta - 1}{3}, \end{cases} \tag{21}$$

$\overline{F_h}$ is the balance tension of the horizontal tie bar, and $\overline{F_v}$ is the balance tension of the vertical tie bar. They can be calculated by the following equation:

$$\begin{cases} \overline{F_h} = \gamma_h \times \left(\overline{K_h}\zeta f_c' A_{str}\right) \times \cos\theta, \\ \overline{F_v} = \gamma_v \times \left(\overline{K_v}\zeta f_c' A_{str}\right) \times \sin\theta, \end{cases} \tag{22}$$

ζ is the softening coefficient of concrete under compression and can be calculated as follows:

$$\zeta \approx \frac{3.35}{\sqrt{f'}}. \tag{23}$$

The main calculation steps of the modified strut-and-tie model are as follows :

(1) Determine relevant parameters of nodes: b_b, b_c, h_b, h_c, h_b'', h_c'', A_{th}, A_{tv}, and f_c'.

Considering that all the stirrups at the joints do not yield when the joints fail, the joint area is simply divided by force. All the area of the stirrups at the middle half participates in the force, while only half of the area of the reinforcing bars at both sides participates in the force [14]. See Figure 14 for specific zones.

The vertical tie bar is composed of the longitudinal bar of the column, and the reinforcement partition of the longitudinal bar participating in the force is shown in Figure 15. It is composed of longitudinal bars of core column and longitudinal bars of rectangular column. According to the stress zone, the calculation method of A_{tv} is as follows:

$$\begin{aligned} A_{tv} &= A_{tvj} + A_{tvx}, \\ \cos\alpha &= \frac{h''/4}{R}, \\ A_{tvx} &= m \times \frac{\pi - 2\alpha}{\pi} \times A_{tvx1} + n \times A_{tvx2}, \end{aligned} \tag{24}$$

where A_{tv} is the effective area of the vertical tie bar, A_{tvj} is the effective area of the longitudinal bars of the rectangular column, A_{tvx} is the effective area of the longitudinal reinforcement of the core column, A_{tvx1} is the effective surface of the longitudinal reinforcement of the outer core column, and A_{tvx2} is the effective area of the longitudinal reinforcement of the inner core column.

(2) Calculate the height a_b of the compression zone of the joint beam cross section (equation (16)).

(3) Calculate the height of the compression zone of the joint column cross section a_c (equation (17)).

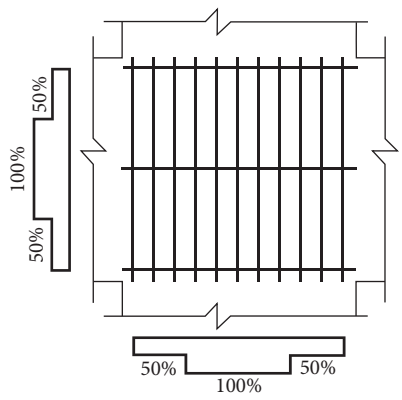

Figure 14: The area partition diagram of the node.

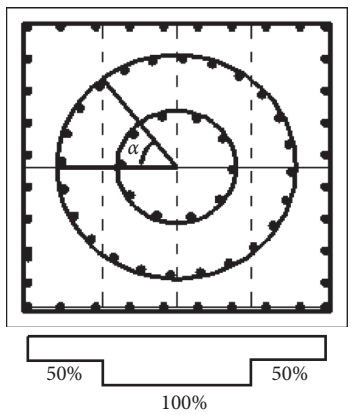

Figure 15: Diagram of column A_{tv} calculation method.

Table 4: The shear force calculation results of each joint are compared with the test results.

Node number	V_j	V_{jh}	V_j/V_{jh}	Average	Standard deviation
BCJ-1	707.25	668.71	1.058		
BCJ-2	975.61	1161.32	0.840	0.965	0.16
BCJ-3	707.25	708.58	0.998		

(4) Calculate the effective height of the baroclinic bar in the joint area (equation (14)).

(5) Calculate the effective width of the baroclinic bar in the joint area is calculated, b_s (equation (15)).

(6) Calculate the softening coefficient ζ of concrete (equation (23)).

(7) Calculate γ_h and γ_v (equation (21)).

(8) Calculate $\overline{K_h}$ and $\overline{K_v}$ (equation (20)).

(9) Calculate $\overline{F_h}$ and $\overline{F_v}$ (equation (22)).

(10) Calculate K_h and K_v (equation (19)).

(11) Calculate K (equation (18)).

(12) Calculate V_j (equation (11)).

The comparison between the calculation results and the test results of the shear capacity of the three multiple composite core column joints (calculated according to the above steps) is shown in Table 4. The average value and standard deviation of the ratio between the calculated value and the measured value are 0.965 and 0.16 respectively. It can be seen that the calculated value of the shear capacity based on the softened tension-compression bar model is in good agreement with the experimental value. The results indicate that it is feasible to use the angle ratio to calculate the effective area of the longitudinal reinforcement of the core column.

5. Conclusion

(1) According to the experimental study, the three specimens of multiple composite core column joints were all damaged by plastic hinge at the beam end, conforming to the seismic design of "strong column and weak beam" and had better seismic performance compared with ordinary beam-column joints.

(2) The hysteresis curves of the joint specimens all show full spindle shape, and the hysteresis loops are relatively full. Increasing the axial compression ratio can significantly improve the initial stiffness and peak load of the joint, while increasing the shear span ratio will lead to a slight decrease in the initial stiffness and peak load.

(3) When the modified softened tension-compression bar model is used to calculate the shear at the joints, a calculation method for the effective area of the vertical tension-compression bar suitable for multiple composite core columns is proposed. Compared with the test results, the model value is slightly lower than the test value, which indicates that the calculation results of this method are safer when designing the shear capacity of frame joints and can provide a theoretical basis for the structural design of practical engineering.

Data Availability

The data used to support the findings of this study are included within the article.

Conflicts of Interest

The authors declare that there are no conflicts of interest regarding the publication of this study.

Acknowledgments

This study was financially supported by the National Natural Science Foundation of China (no. 51868073), and its support is gratefully appreciated.

References

[1] J. Tang, J. Feng, and T. Pang, "Experimental study on shear strength in core area of reinforced concrete frame beam-column joints," *Journal of Nanjing Institute of Technology*, vol. 31, no. 4, pp. 61–75, 1985.

[2] J. Fu, "Experimental study on seismic behavior of reinforced concrete frame joints considering axial compression ratio," *Journal of Chongqing Jianzhu University*, vol. 22, no. Z1, pp. 60–66, 2000.

[3] W. Wang, J. Xue, H. Zhang et al., "Seismic damage analysis of frame structure in 5.12 Wenchuan earthquake and its seismic implications," *World Earthquake Engineering*, vol. 25, no. 4, pp. 131–135, 2009.

[4] G. Wang, X. Qin, D. Han, and Z. Liu, "Study on seepage and deformation characteristics of coal microstructure by 3D reconstruction of CT images at high temperatures," *International Journal of Mining Science and Technology*, vol. 31, no. 2, pp. 175–185, 2021.

[5] Y. Zhang, Y. Xie, Y. Zhang, J. Qiu, and S. Wu, "The adoption of deep neural network (DNN) to the prediction of soil liquefaction based on shear wave velocity," *Bulletin of Engineering Geology and the Environment*, vol. 80, no. 6, pp. 5053–5060, 2021.

[6] S. Shao, C. Wu, H. Min et al., "A novel coating technology for fast sealing of air leakage in underground coal mines," *International Journal of Mining Science and Technology*, vol. 31, no. 2, pp. 313–320, 2021.

[7] Y.-G. Zhang, J. Qiu, Y. Zhang, and Y. Wei, "The adoption of ELM to the prediction of soil liquefaction based on CPT," *Natural Hazards*, vol. 107, 2021.

[8] H. Rafezi and F. Hassani, "Drilling signals analysis for tricone bit condition monitoring," *International Journal of Mining Science and Technology*, vol. 31, no. 2, pp. 187–195, 2021.

[9] Y. Zhang, J. Qiu, Y. Zhang, and Y. Xie, "The adoption of a support vector machine optimized by GWO to the prediction of soil liquefaction," *Environmental Earth Sciences*, vol. 80, no. 9, 2021.

[10] H. Zhao, T. Ren, and A. Remennikov, "A hybrid tubular standing support for underground mines: compressive behaviour," *International Journal of Mining Science and Technology*, vol. 31, no. 2, pp. 215–224, 2021.

[11] Y.-G. Zhang, J. Tang, Z.-Y. He, J. Tan, and C. Li, "A novel displacement prediction method using gated recurrent unit model with time series analysis in the Erdaohe landslide," *Natural Hazards*, vol. 105, no. 1, pp. 783–813, 2020.

[12] P. An, W. Xia, Y. Peng, and G. Xie, "Comparative filtration and dewatering behavior of vitrinite and inertinite of bituminous coal: experiment and simulation study," *International Journal of Mining Science and Technology*, vol. 31, no. 2, pp. 233–240, 2021.

[13] Y. You, J. Fu, S. Bai et al., "A new recognition of the calculation formula of shear capacity of seismic reinforced concrete frame joints," *Journal of Chongqing Jianzhu University*, vol. 41, no. 1, pp. 18–29, 1997.

[14] G. Xing, *Research on Failure Mechanism and Design Method of Interior Joint with Different Depth Beams in RC Frame Structure*, Chang'an University, Xi'an, China, 2010.

[15] G. Xing, Z. He, D. Niu et al., "Analytical model for shear strength of reinforced concrete beam-column-slab exterior joints," *Journal of Central South University*, vol. 45, no. 9, pp. 3277–3282, 2014.

[16] G. Xing, L. I. U. Bo-quan, and N. Di-tao, "Shear strength of reinforced concrete frame joints using modified softened strut-and-tie model," *Engineering Mechanics*, vol. 30, no. 8, pp. 60–66, 2013.

[17] S. J. Hwang and H. J. Lee, "Analytical model for predicting shear strengths of interior reinforced concrete beam-column joints for seismic resistance," *ACI Structural Journal*, vol. 97, no. 1, pp. 35–44, 2000.

[18] S. J. Hwang and H. J. Lee, "Analytical model for predicting shear strengths of exterior reinforced concrete beam-column joints for seismic resistance," *ACI Structural Journal*, vol. 96, no. 5, pp. 846–857, 1999.

[19] J. Yang, *Study on Seismic Performance of High-Strength Concrete Columns with Multiple Composite Central Reinforcement*, Chang'an University, Xi'an, China, 2019.

[20] M. Wakabayashi, K. Minami, Y. Nishimura et al., *Anchorage of Bent Bar in Reinforced Concrete Exterior Joints*, Japan Concrete Institute, Tokyo, Japan, 1983.

[21] H. Omine, I. Sadamura, H. Yashiro et al., *Study on the Strengthening of Reinforced concrete Columns by central Reinforcing Steel Element*, Architectural Institute of Japan, Tokyo, Japan, 1999.

[22] H. Kadoya, J. Kawaguchi, and S. Morino, *Experimental Study On Strength And Stiffness of Bare Type CFT Column Base With Central Reinforcing Bars*, American Society of Civil Engineers, Reston, VA, USA, 2006.

[23] Framework Node Thematic Research Group, "Experimental study on shear strength of core area of reinforced concrete frame beam-column joints under low cyclic load," *Journal of Building Structures*, vol. 4, no. 6, pp. 1–17, 1983.

[24] B. Liu, S. Huang, A. Zhou et al., "Experimental study on seismic behavior of eccentric beam-column joints in reinforced concrete frames," *Journal of Building Structures*, vol. 20, no. 5, pp. 50–58, 1999.

[25] Q. Zheng, E. Fang, C. Ke et al., "Experimental study on seismic behavior of reinforced concrete large eccentric beam-column joints," *Journal of Building Structures*, vol. 20, no. 6, pp. 2–10, 1999.

[26] S.-J. Hwang and H.-J. Lee, "Strength prediction for discontinuity regions by softened strut-and-tie model," *Journal of Structural Engineering*, vol. 128, no. 12, pp. 1519–1526, 2002.

[27] D. Gao, K. Shi, and S. Zhao, "Calculation method for shear capacity of steel fiber reinforced concrete beam-column joints based on softened strut-and-tie model," *Journal of Civil Engineering*, vol. 47, no. 9, pp. 101–109, 2014.

[28] GB/T50081-2019, *Standard for Test Methods of Concrete Physical and Mechanical Properties*, National Standard of the People's Republic of China, China Building Industry Press, Beijing, China, 2019.